

Two-fluid dynamics in driven $\text{YBa}_2\text{Cu}_3\text{O}_{6.48}$ A. Ribak^{1,*}, M. Buzzi¹, D. Nicoletti¹, R. Singla¹, Y. Liu², S. Nakata², B. Keimer², and A. Cavalleri^{1,3,†}¹Max Planck Institute for the Structure and Dynamics of Matter, 22761 Hamburg, Germany²Max Planck Institute for Solid State Research, 70569 Stuttgart, Germany³Department of Physics, Clarendon Laboratory, University of Oxford, Oxford OX1 3PU, United Kingdom

(Received 14 October 2022; accepted 1 March 2023; published 13 March 2023)

Coherent optical excitation of certain phonon modes in $\text{YBa}_2\text{Cu}_3\text{O}_{6+x}$ has been shown to induce superconducting-like interlayer coherence at temperatures higher than T_c . Recent work has associated these phenomena to a parametric excitation and amplification of Josephson plasma polaritons, which are overdamped above T_c but are made coherent by the phonon drive. However, the dissipative response of uncondensed quasiparticles, which do not couple in the same way to the phonon drive, has not been addressed. Here, we investigate both the enhancement of the superfluid density, $\omega\sigma_2(\omega)$, and the dissipative response of quasiparticles, $\sigma_1(\omega)$, by systematically tuning the duration and energy of the mid-infrared pulse while keeping the peak field fixed. We find that the photoinduced superfluid density saturates to the zero-temperature equilibrium value for pulses made longer than the phonon dephasing time, while the dissipative component continues to grow with increasing pulse duration. We show that superfluid and dissipation remain uncoupled as long as the drive is on, and identify an optimal regime of pump pulse durations for which the superconducting response is maximum and dissipation is minimized.

DOI: [10.1103/PhysRevB.107.104508](https://doi.org/10.1103/PhysRevB.107.104508)**I. INTRODUCTION**

When cooled below the equilibrium superconducting transition, cuprate superconductors acquire a characteristic terahertz-frequency optical response, reflecting coherent interlayer transport and condensation of normal state quasiparticles [1–4]. These features are displayed in Figs. 1(a) and 1(b), where we report the complex optical conductivity of underdoped $\text{YBa}_2\text{Cu}_3\text{O}_{6+x}$ along the c axis for $T > T_c$ (red) and $T < T_c$ (blue). In the normal state, the real (dissipative) part of the conductivity, $\sigma_1(\omega)$, at low frequencies ($\omega \leq 100 \text{ cm}^{-1}$) is finite, exhibiting a flat and featureless spectrum [red curve in Fig. 1(a), left panel]. For $\omega > 100 \text{ cm}^{-1}$ [Fig. 1(a), right panel] a collection of narrow absorption peaks is observed, assigned to infrared-active phonons, along with a broader contribution around 400 cm^{-1} , which has been attributed to the so-called “transverse Josephson plasmon” [5–8]. Notably, unlike in conventional superconductors, the spectral weight loss across the superconducting transition (blue shading) extends over a frequency range which is far broader than the superconducting gap, a behavior which is commonly found in strongly correlated superconductors [1–4,9]. The presence of a zero-frequency pole in $\sigma_1(\omega)$ manifests itself in the imaginary (inductive) part of the optical conductivity, $\sigma_2(\omega)$, as a

$1/\omega$ divergence at low frequency [Fig. 1(b)], which allows the determination of the superfluid density from finite frequency measurements, as $\lim_{\omega \rightarrow 0} \omega\sigma_2(\omega) = \frac{n_s e^2}{m}$ (here n_s is the superfluid density, e the electron charge, and m the electron mass).

In a recent series of experiments, femtosecond mid-infrared pulses have been used to resonantly excite apical oxygen vibrations in underdoped $\text{YBa}_2\text{Cu}_3\text{O}_{6+x}$ [10–16]. These studies revealed a light-induced transient optical response featuring a finite light induced superfluid density, as seen most directly in the transient $\sigma_2(\omega)$ which acquires the same $1/\omega$ behavior observed below T_c . Strikingly, these effects were observed all the way up to the pseudogap temperature, T^* [10–13]. A representative result is reported in Figs. 1(c) and 1(d), where we show the complex optical conductivity of $\text{YBa}_2\text{Cu}_3\text{O}_{6.48}$ measured at $T = 100 \text{ K} \approx 2T_c$ before (red lines) and after (blue circles) mid-infrared photoexcitation (here, the region covered by the pump spectrum is shaded in blue). Notably, this analogy does not apply to the real part of optical conductivity. In the transient state the low-frequency $\sigma_1(\omega)$ shows an increase [Fig. 1(c), left panel], as opposed to a decrease upon cooling [Fig. 1(a), left panel]. This dissipative response can be reproduced by fitting the data with a two-fluid model in which a superconducting term, given by a Josephson plasma resonance, coexists with an overdamped Drude absorption [12,17–19] that accounts for the tunneling of incoherent normal carriers [dashed lines in Figs. 1(c) and 1(d); see Appendix D for details on the fitting model].

Recently, further experimental and theoretical work [20,21] has provided evidence that periodic driving of the apical oxygen modes acts as a parametric pump for the amplification of incoherent Josephson plasmons in the

*amit.ribak@mpsd.mpg.de

†andrea.cavalleri@mpsd.mpg.de

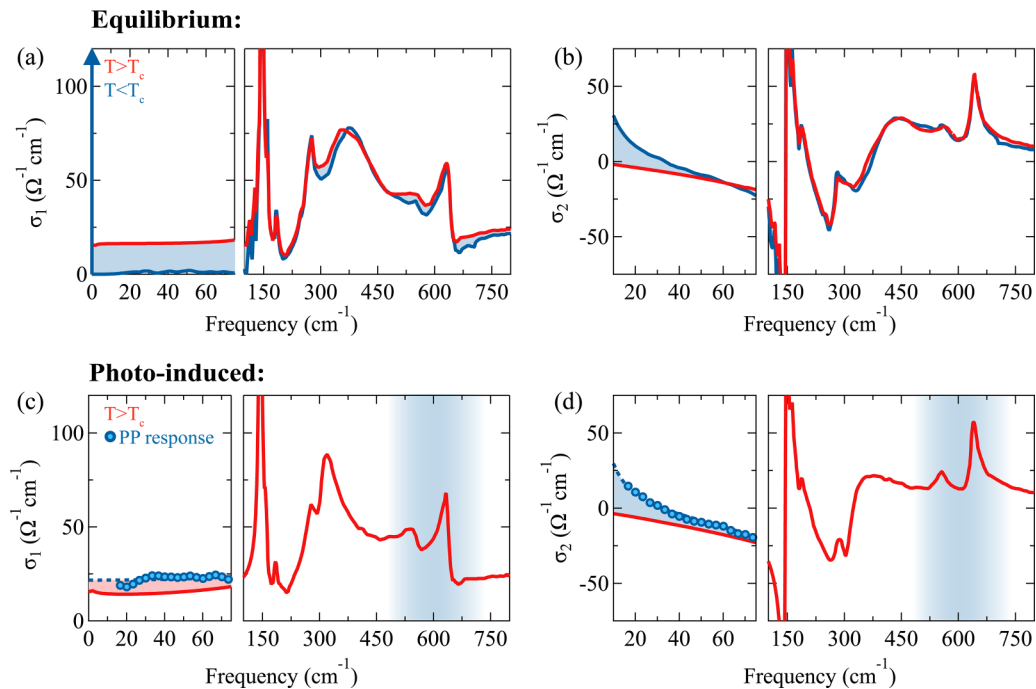


FIG. 1. (a), (b) Complex c -axis optical conductivity, $\sigma_1(\omega) + i\sigma_2(\omega)$, of underdoped $\text{YBa}_2\text{Cu}_3\text{O}_{6+x}$ across the equilibrium superconducting transition. Data at $T = 60 \text{ K} > T_c$ (red) and $T = 10 \text{ K} < T_c$ ($T_c = 52 \text{ K}$) are reported [2,11]. Shaded blue regions represent the changes in the spectra across T_c . The vertical arrow in (a) is a pole at zero frequency indicative of dissipationless transport. (c), (d) Same quantities as in (a) and (b) measured in $\text{YBa}_2\text{Cu}_3\text{O}_{6.48}$ at $T = 100 \text{ K}$ before (red) and after (blue circles) mid-infrared photoexcitation (see Sec. II). Red and blue shadings in (c) and (d) represent photoinduced changes in the spectra, while the shaded blue area around 600 cm^{-1} indicates the frequency range covered by the mid-infrared pump. Dashed blue lines are fits to the transient optical conductivity performed with a model including a Josephson plasmon and a Drude term (see also Appendix D).

pseudogap phase, giving rise to the superconducting-like optical properties observed with THz spectroscopy. In this context, it is not clear how sustained drives affect the dissipative response, and how the ratio of superfluid density to dissipative heating can be optimized. Here, we explore this issue by photoexciting $\text{YBa}_2\text{Cu}_3\text{O}_{6.48}$ with mid-infrared pump pulses of variable duration, tuned to resonantly drive the same 570 cm^{-1} and 670 cm^{-1} apical oxygen phonons that induce the superconducting-like behavior discussed above [11,12].

II. EXPERIMENT

Single crystals of $\text{YBa}_2\text{Cu}_3\text{O}_{6.48}$ with typical dimensions of $1.5 \times 1.5 \times 0.4 \text{ mm}^3$ were mounted to expose a surface determined by the out-of-plane ($\parallel c$) and one of the in-plane ($\perp c$) crystallographic directions. The crystals were photoexcited using mid-infrared pump pulses generated using an optical parametric amplifier pumped by a commercial Ti:sapphire laser system. These pump pulses were polarized along the c axis and made to propagate through dispersive, optically polished NaCl plates before impinging on the sample. This yielded excitation pulses with the same spectral content but duration varying from 150 fs up to 4.3 ps. Broadband THz probe pulses ($\approx 17\text{--}75 \text{ cm}^{-1}$) were generated using a photoconductive antenna from the direct output of the Ti:sapphire amplifier. These THz probe pulses, with polarization parallel to the crystal c axis, were then focused on the sample and detected by electro-optical sampling after reflection in a $500 \mu\text{m}$ thick ZnTe (110) crystal, yielding the photoinduced

changes in the low-frequency complex reflection coefficient $\tilde{r}(\omega)$ as a function of pump-probe time delay. The penetration depth of the mid-infrared pump ($\approx 1 \mu\text{m}$) was shorter than that of the THz probe ($5\text{--}10 \mu\text{m}$). This was taken into account by modeling the sample as a multilayered photoexcited stack on top of an unperturbed bulk in order to obtain the optical response functions corresponding to an effective semi-infinite and homogeneously excited medium (see Appendix C and Ref. [22]). The measurements presented in the following were carried out at a constant peak field of 2.2 MV/cm for all pulse durations.

III. RESULTS

Figure 2 provides a visual summary of the results of the pulse duration dependence, for which we report extended data sets in Appendix E. The color plots show the frequency- and time-dependent transient complex optical conductivity $\sigma_1(\omega) + i\sigma_2(\omega)$ after excitation with different mid-infrared pulse durations varying from 0.15 ps to 4.3 ps at a temperature $T = 100 \text{ K} \gg T_c (\cong 52 \text{ K})$. The $\sigma_1(\omega)$ spectra show an almost frequency-independent increase (red colors) at all positive time delays which is indicative of enhanced dissipation. The imaginary conductivity, $\sigma_2(\omega)$, displays instead a $1/\omega$ -like divergence at low frequency (blue shaded areas), which persists for a time window of the order of the pump pulse duration. Besides the new observation of an increased lifetime of the transient superconducting response, our data are consistent with the previous findings reported in Refs. [10–12]. How-

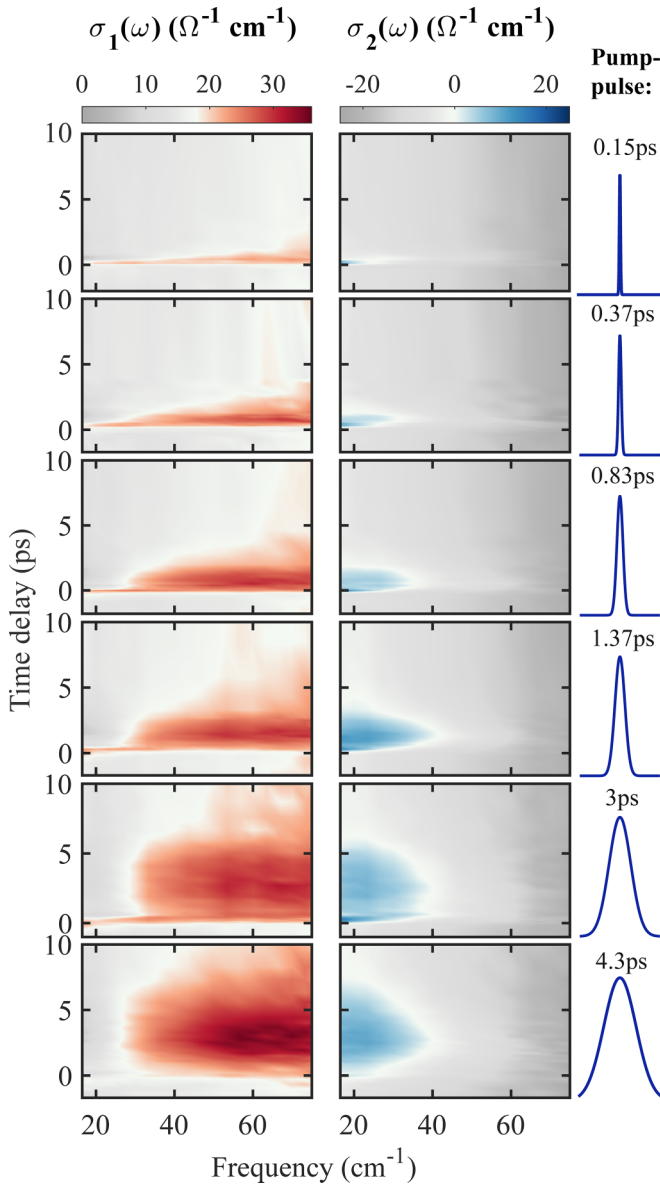


FIG. 2. Frequency- and time-delay-dependent complex optical conductivity of $\text{YBa}_2\text{Cu}_3\text{O}_{6.48}$ after photoexcitation with different mid-infrared pump pulse duration at $T = 100$ K. The peak field was kept constant at 2.2 MV/cm for all measurements.

ever, while the qualitative features in the optical spectra do not depend on the drive pulse duration, we find quantitative differences, analyzed in the following.

To reconstruct the dynamical evolution of the two components of the transient response, namely the dissipative one in $\sigma_1(\omega)$ and the coherent one in $\sigma_2(\omega)$, we extracted two representative quantities from the individual THz spectra measured at each time delay.

The transient $\sigma_1(\omega)$ spectral weight, indicative of dissipation, is determined as $\int_{20 \text{ cm}^{-1}}^{75 \text{ cm}^{-1}} \sigma_1(\omega) d\omega$, while the coherent response is expressed as $\lim_{\omega \rightarrow 0} \omega \sigma_2(\omega)$, which in a superconductor at equilibrium is proportional to the superfluid density. Figures 3(a)–3(b) and 3(c)–3(d) display these two figures of merit for representative pulse durations of 0.15 ps and 3 ps, respectively. For both data sets, after photoexcitation the $\sigma_1(\omega)$

spectral weight is enhanced and then relaxes on a timescale that clearly exceeds the pump pulse duration. A different evolution is observed instead in $\lim_{\omega \rightarrow 0} \omega \sigma_2(\omega)$, which appears to be finite only while the system is driven [blue shading in Figs. 3(c) and 3(d)]. In this case, excitation with longer pulses allows the “zero-temperature” equilibrium superfluid density to be reached. This is reported for comparison as a dashed horizontal line in Fig. 3(d). A more accurate visualization of how the lifetime of the photoinduced superconducting state scales with the pump pulse duration is displayed in Fig. 3(e), emphasizing a one-to-one correspondence between drive duration and lifetime.

The transient $\sigma_1(\omega)$ spectral weight and $\lim_{\omega \rightarrow 0} \omega \sigma_2(\omega)$ can be compared to their respective values in equilibrium at different temperatures to extract a “quasitemperature” of these two fluids, which we also provide in Figs. 3(a)–3(b) and 3(c)–3(d). Unlike in the equilibrium superconductor, in this driven state some normal quasiparticles remain and are heated up by the pump up to an apparent temperature of ≈ 300 K, while the parametric drive appears to synchronize preexisting Cooper pairs yielding an effective superfluid quasitemperature of ≈ 10 K.

In Fig. 4 we display the same quantities as in Figs. 3(a)–3(d) as a function of pump pulse duration, measured at the peak of the response, in order to study how the dissipative and superfluid components are affected by prolonged driving. Our data reveal that, while the normal dissipative part increases monotonically with the pump duration [Fig. 4(a)] with no sign of saturation, the coherent superconducting part [Fig. 4(b)] saturates almost exactly at the equilibrium value of the superfluid density measured below T_c . The pulse duration at which saturation sets in matches closely the lifetime of the resonantly excited apical oxygen vibration, as estimated from both the linewidth of the absorption peak in the conductivity spectrum [3] and the decay time of coherently driven oscillations in the mid-infrared pump / second harmonic probe experiment of Ref. [20].

IV. DISCUSSION

We studied how optically stimulated superconductivity appears in $\text{YBa}_2\text{Cu}_3\text{O}_{6.48}$ after photoexcitation with driving pulses of variable duration and constant peak electric field. Especially in the context of parametrically amplified superconductivity [20–24], such a field-dependent investigation allowed us to map out the interplay between coherent response and dissipation in the photoinduced state.

As the duration of the drive pulses increases, the transient spectral features and their lifetime show peculiar behaviors. Namely, while the $\sigma_1(\omega)$ spectral weight grows monotonically, the photoinduced superfluid density extracted from $\sigma_2(\omega)$ increases progressively only for pump pulse durations up to ≈ 1 ps and then saturates to the value measured at equilibrium at $T = 10$ K.

The pulse duration dependence reported here is fully consistent with the scenario proposed in Refs. [20,21], where excitation of the apical-oxygen phonon mode in $\text{YBa}_2\text{Cu}_3\text{O}_{6.48}$ induces superconducting coherences by parametric amplification of incoherent Josephson plasmons that are already present above T_c . With increasing pump pulse

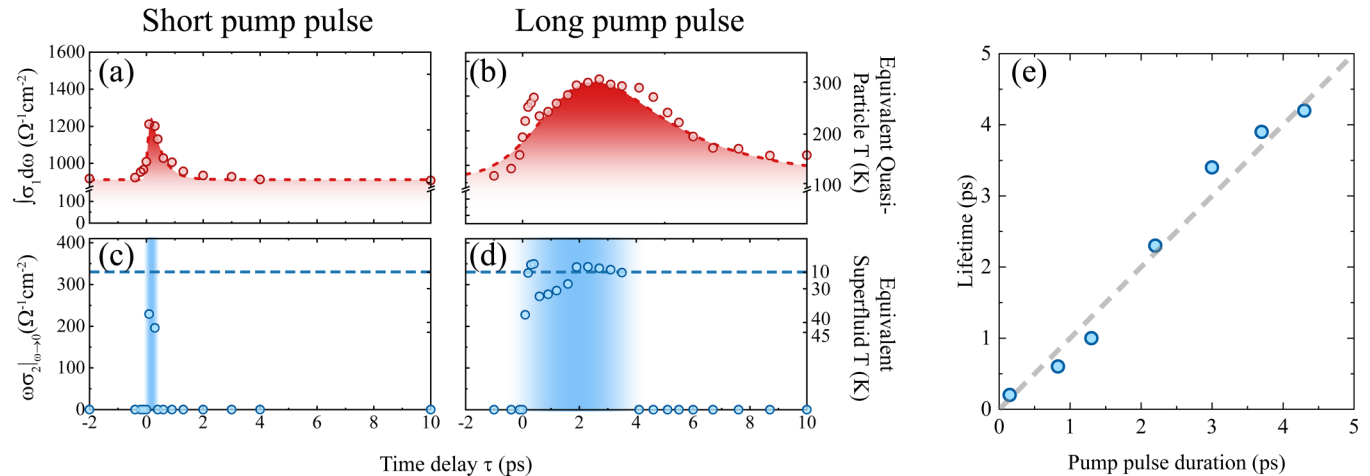


FIG. 3. (a), (b) Dynamical evolution of the transient spectral weight, $\int_{20 \text{ cm}^{-1}}^{75 \text{ cm}^{-1}} \sigma_1(\omega) d\omega$, indicative of dissipation, as a function of pump-probe time delay τ , for unstretched (0.15 ps) and stretched (3 ps) excitation. The dashed line is a fit to the data with a finite rise time and an exponential decay. (c), (d) Corresponding evolution of the coherent superconducting-like response, $\lim_{\omega \rightarrow 0} \omega \sigma_2(\omega)$. The horizontal lines indicate the 10 K equilibrium value of the superfluid density, while the shaded blue area represents the time delay window for which a finite coherent response is detected. Equivalent quasitemperatures (see Sec. III) are reported on the right axes. (e) Lifetime of the photoinduced superconducting state, estimated from the width of the shaded regions in (c) and (d), as a function of pump pulse duration.

duration at constant peak field, the oscillation amplitude of the driven apical oxygen mode grows progressively and saturates for pulse durations comparable to the mode lifetime (estimated to be ≈ 1 ps, in Sec. III). Following the arguments in Refs. [20,21], a saturation of the parametric drive amplitude implies that the light-induced superfluid density should stop increasing, as observed experimentally in Fig. 4(b).

We now turn to the the monotonic increase of the $\sigma_1(\omega)$ spectral weight with increasing pulse duration, without any signs of saturation. We rationalize this behavior by observing how, while the peak field is kept constant, as the pump pulse duration grows its fluence increases (Fig. 4), making the direct excitation of quasiparticles more effective. We speculate that this dissipative channel develops along the nodal directions of the Brillouin zone while the coherent response involves the antinodal regions of the pseudogap.

Another characteristic of the transient state is that its lifetime increases for progressively longer drive pulses, while never exceeding the duration of the pump itself [see Fig. 3(e)]. Such behavior implies that the light-induced superconducting state in $\text{YBa}_2\text{Cu}_3\text{O}_{6.48}$ lacks intrinsic coherence and persists only while the drive is on. This is unlike the coherent response found in vibrationally stimulated K_3C_{60} , which persists for timescales far longer than the pump pulse [25,26].

These observations underscore how the dynamics of synchronized superfluid and heated quasiparticles is uncorrelated as long as the drive is on. Our interpretation assumes preexisting electron pairs without phase coherence. The possible creation of new pairs appears unlikely, as the transient superfluid density never exceeds the equilibrium value. Finally, our measurement allows us to identify an ideal excitation regime, one with drive pulses of the order of 1 ps, for which the superconducting-like response reaches the “zero-temperature” value of the superfluid density and is maximized in comparison to the dissipative component, thus indicating a

path for optimizing light-induced superconductivity in bilayer cuprates.

ACKNOWLEDGMENTS

The research leading to these results received funding from the European Research Council under the European Union’s Seventh Framework Programme (FP7/2007-2013)/ERC Grant Agreement No. 319286 (QMAC). We acknowledge support from the Deutsche Forschungsgemeinschaft (DFG; German Research Foundation) via the excellence cluster “CUI: Advanced Imaging of Matter” (EXC 2056, project ID 390715994) and the priority program SFB925 (Project ID 170620586).

APPENDIX A: SAMPLE GROWTH AND CHARACTERIZATION

$\text{YBa}_2\text{Cu}_3\text{O}_{6.48}$ crystals of typical dimensions $1.5 \times 1.5 \times 0.4$ mm were grown in Y-stabilized zirconium crucibles. The hole doping of the Cu-O planes was adjusted by controlling the oxygen content of the Cu-O chain layer by annealing in flowing O_2 and subsequent rapid quenching. A sharp superconducting transition at $T_c = 55$ K ($\Delta T_c \approx 2$ K) was determined by dc magnetization measurements, as shown in Fig. 5.

APPENDIX B: EXPERIMENTAL SETUP AND DATA ACQUISITION

To retrieve the photoinduced changes in the optical properties of $\text{YBa}_2\text{Cu}_3\text{O}_{6.48}$ we performed a series of mid-infrared pump / THz probe experiments with different pump pulse durations (see Fig. 6). The $\text{YBa}_2\text{Cu}_3\text{O}_{6.48}$ crystals were manually polished in order to expose a surface which contained both an in-plane and an out-of-plane axis. They were glued on top of cutting-edge-shaped holders to prevent stray reflections

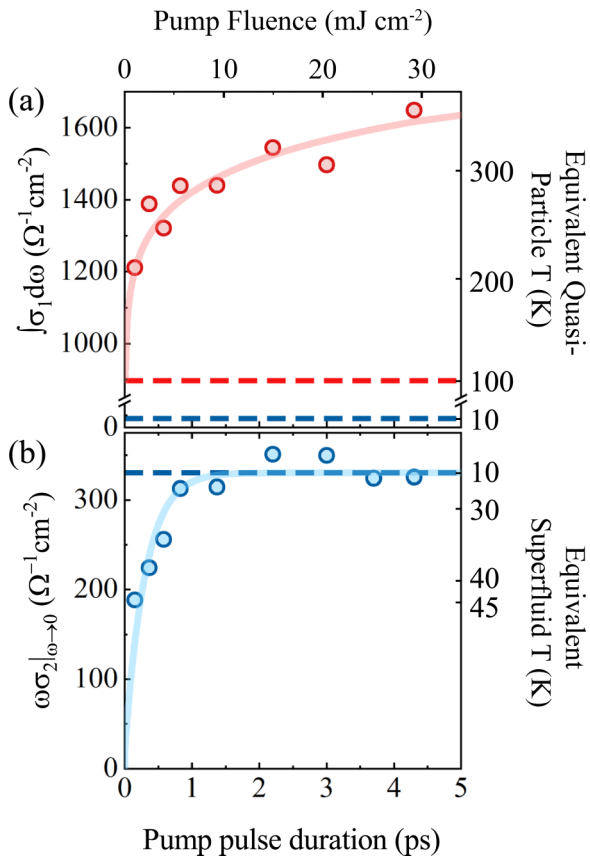


FIG. 4. (a) Evolution of the transient spectral weight, $\int_{20 \text{ cm}^{-1}}^{75 \text{ cm}^{-1}} \sigma_1(\omega) d\omega$, and (b) of the coherent superconducting-like response, $\lim_{\omega \rightarrow 0} \omega \sigma_2(\omega)$, measured at the time delay corresponding to the peak of the response, as a function pump pulse duration. The top horizontal axis indicates the pump fluence which increases linearly with the pump pulse duration to keep the peak electric field constant. The red and blue horizontal dashed lines in (a) indicate the equilibrium spectral weight values at $T = 100$ K and $T = 10$ K, respectively, while that in (b) refers to the equilibrium superfluid density at $T = 10$ K. Equivalent temperatures are reported on the right axes (see discussion in Sec. III and Sec. IV).

from interfering with the signal from the sample surface. These holders were installed on the cold finger of a He-flow cryostat to allow for temperature control.

$\text{YBa}_2\text{Cu}_3\text{O}_{6.48}$ was photoexcited with mid-infrared pump pulses of duration variable between 150 fs and 4.3 ps, tuned to ~ 20 THz center frequency, in resonance to the B_{1u} phonon modes that were previously shown to enhance interlayer superconducting coupling.

These pump pulses were generated by difference frequency mixing of the signal and idler outputs of an optical parametric amplifier (OPA) in a 0.4 mm thick GaSe crystal which yielded 20-THz-center-wavelength pulses with total energy of $\sim 50 \mu\text{J}$ and typical duration of 150 fs. The OPA was pumped with ~ 35 fs long pulses from a commercial Ti:sapphire regenerative amplifier (800 nm wavelength). The duration of the pump pulses was controlled by introducing dispersion through propagation in NaCl rods and their intensity was adjusted using two freestanding wire-grid polarizers to keep the peak electric field constant at 2.2 MV/cm.

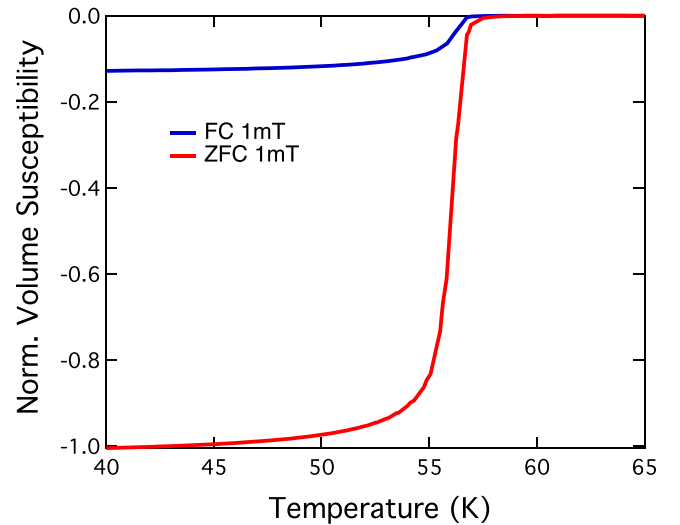


FIG. 5. SQUID characterization of the DC magnetization (ZFC: zero field cooled, FC: field cooled) across the superconducting transition.

The pump pulses were then focused onto the sample surface, with their polarization aligned with the c axis of the $\text{YBa}_2\text{Cu}_3\text{O}_{6.48}$ crystal. The typical pump spot size was ~ 0.5 mm allowing for a homogenous illumination of the

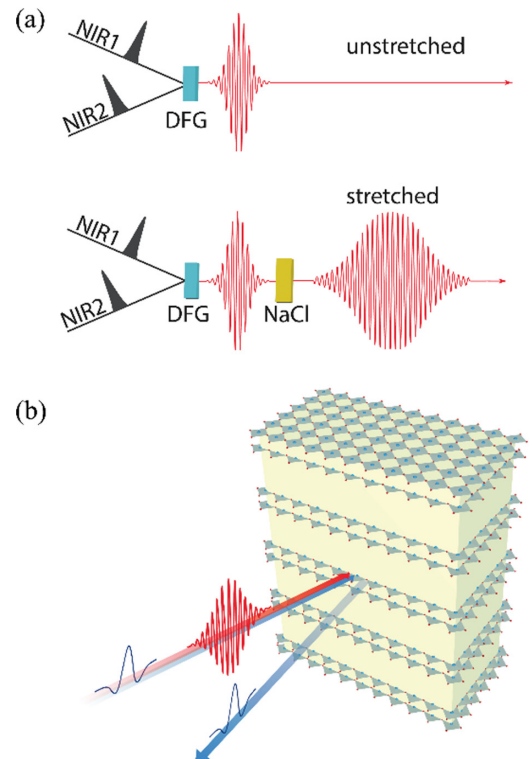


FIG. 6. Pump-probe experimental setup. (a) The signal and idler outputs from an optical parametric amplifier are sent to a GaSe crystal for difference frequency generation (DFG). The duration of these pulses can be controlled by letting them propagate through optically polished NaCl plates. (b) The MIR pump pulse (red) and the single-cycle THz probe (blue) are polarized along the c axis of $\text{YBa}_2\text{Cu}_3\text{O}_{6.48}$.

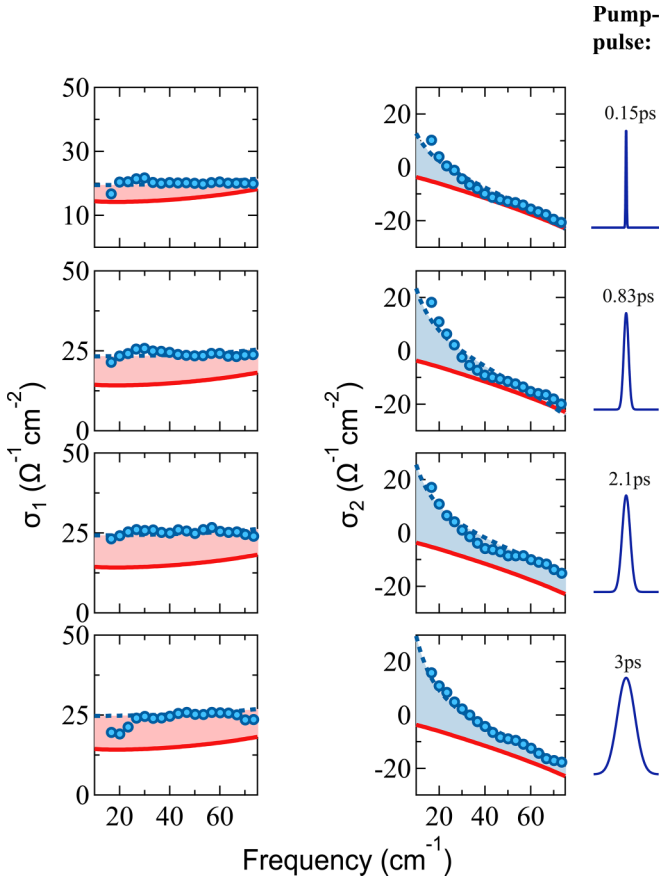


FIG. 7. Complex c -axis optical conductivity, $\sigma_1(\omega) + i\sigma_2(\omega)$, measured in $\text{YBa}_2\text{Cu}_3\text{O}_{6.48}$ at $T = 100$ K in equilibrium (red) and at one selected pump-probe time delay after photoexcitation (blue circles), corresponding to the peak of the coherent, superconducting-like response. We display data for different mid-infrared pump pulse durations (shown on the right), all taken with the same peak field of 2.2 MV/cm. Dashed blue lines are fits performed with a model including a Josephson plasmon and a Drude term (see Appendix D). This data set was used to produce the color plots in Fig. 2.

probed area. A maximum fluence of ~ 30 mJ/cm² could be achieved, allowing us to maintain a 2.2 MV/cm peak field at the longest pulse duration of 4.3 ps.

The transient reflectivity changes after photoexcitation were retrieved via time-domain THz spectroscopy using single-cycle THz pulses generated by illuminating a commercial photoconductive antenna with 800 nm pulses. These probe pulses, polarized along the c axis of the $\text{YBa}_2\text{Cu}_3\text{O}_{6.48}$ crystal, were focused at normal incidence onto the sample surface on a spot of $\lesssim 0.3$ mm diameter. After reflection from the sample surface, their electric field was detected via electro-optic sampling in a 500 μm thick optically contacted ZnTe crystal. This setup provided a spectral bandwidth extending from ~ 17 to 75 cm^{-1} .

In order to minimize the effects on the pump-probe time resolution due to the finite duration of the THz probe pulse, we performed the experiment as described in Ref. [27]. The transient reflected field at each time delay τ after excitation was obtained by keeping fixed the delay τ between the pump pulse and the electro-optic sampling gate pulse, while scan-

ning the delay t of the single-cycle THz probe pulse. The stationary probe electric field $E_R(t)$ and the differential electric field $\Delta E_R(t, \tau)$ reflected from the sample were recorded simultaneously by feeding the electro-optic sampling signal into a digitizer that sampled individual laser pulses, and mechanically chopping the pump and probe beams at different frequencies. $E_R(t)$ and $\Delta E_R(t, \tau)$ were then independently Fourier transformed to obtain the complex-valued, frequency-dependent $\tilde{E}_R(\omega)$ and $\Delta \tilde{E}_R(\omega, \tau)$.

APPENDIX C: DETERMINATION OF THE TRANSIENT OPTICAL PROPERTIES

From the frequency-dependent measured quantities $\tilde{E}_R(\omega)$ and $\Delta \tilde{E}_R(\omega, \tau)$ the complex reflection coefficient in the photoexcited state could be extracted by inverting the following equation:

$$\frac{\Delta \tilde{E}_R(\omega, \tau)}{\tilde{E}_R(\omega)} = \frac{\tilde{r}_{\text{pumped}}(\omega, \tau) - \tilde{r}_0(\omega)}{\tilde{r}_0(\omega)}. \quad (\text{C1})$$

The penetration depth (~ 0.7 μm) of the excitation pulses (defined as $d(\omega) = \frac{c}{2\omega} \text{Im}[\tilde{n}_0(\omega)]$, where $\tilde{n}_0(\omega)$ is the equilibrium complex refractive index) was typically smaller than that of the probe pulses (5–10 μm). Due to this, the probed volume was not homogeneously excited and this was taken into account using the following approach.

As the pump penetrates the material, its intensity is reduced and will induce progressively weaker changes in the refractive index of the sample. We modeled this condition by “slicing” the probed thickness of the material into thin layers, where we assumed that the pump-induced changes in the refractive index were proportional to the pump intensity in the layer, i.e., $\tilde{n}(\omega, z) = \tilde{n}_0(\omega) + \Delta \tilde{n}(\omega)e^{-\alpha z}$. Here, $\tilde{n}_0(\omega)$ is the equilibrium complex refractive index, α is the attenuation coefficient at the pump frequency, and z is the spatial coordinate along the sample thickness.

For each probe frequency ω , the complex reflection coefficient $\tilde{r}(\Delta \tilde{n})$ of such a multilayer stack was calculated with a characteristic matrix approach [28], keeping $\Delta \tilde{n}$ as a free parameter. Equation (C1) relates the measured quantity $\frac{\Delta \tilde{E}_R(\omega, \tau)}{\tilde{E}_R(\omega)}$ to the changes in the complex reflection coefficient. One can extract $\Delta \tilde{n}$ by minimizing numerically:

$$\left| \frac{\Delta \tilde{E}_R(\omega, \tau)}{\tilde{E}_R(\omega)} - \frac{\tilde{r}(\omega, \Delta \tilde{n}) - \tilde{r}_0(\omega)}{\tilde{r}_0(\omega)} \right|. \quad (\text{C2})$$

The value of $\Delta \tilde{n}(\omega)$ retrieved by this minimization represents the pump-induced change in the refractive index at the surface. By taking $\tilde{n}(\omega) = \tilde{n}_0(\omega) + \Delta \tilde{n}(\omega)$, one can reconstruct the optical response functions of the material as if it had been homogeneously transformed by the pump.

APPENDIX D: DATA ANALYSIS AND FITTING MODELS

At each pump-probe time delay τ , the transient c -axis optical response functions were fitted with a two-fluid model including the response of a Josephson plasma and a Drude contribution, to account for dissipation arising from residual quasiparticles [12, 19]. In addition to this, the phonon modes in the mid-infrared ($150 \text{ cm}^{-1} \lesssim \omega \lesssim 700 \text{ cm}^{-1}$) and the high-frequency electronic absorption ($\omega \gtrsim 3000 \text{ cm}^{-1}$) were

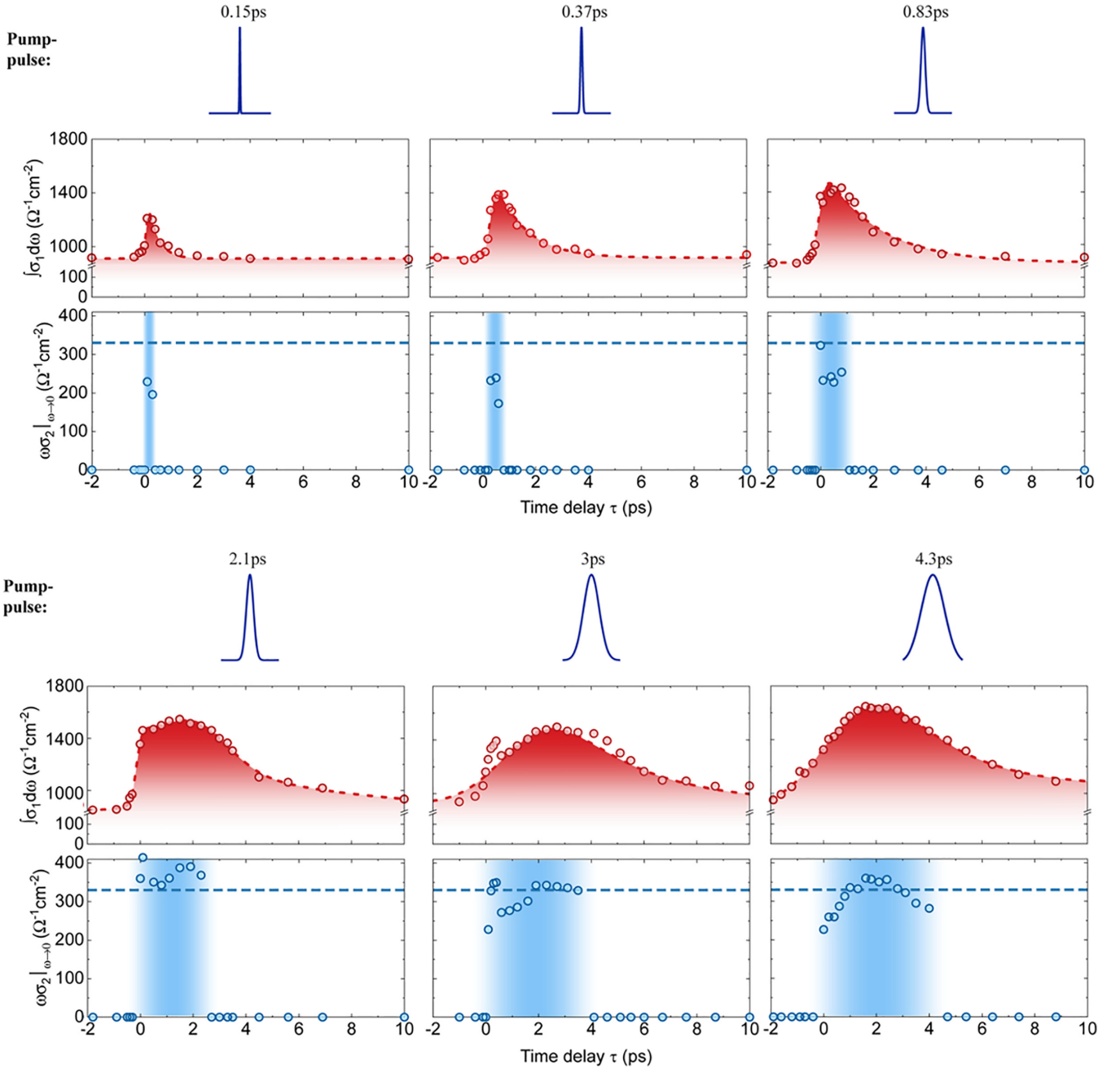


FIG. 8. Dynamical evolution of the transient spectral weight, $\int_{20 \text{ cm}^{-1}}^{75 \text{ cm}^{-1}} \sigma_1(\omega) d\omega$, indicative of dissipation, and of the coherent superconducting-like response, $\lim_{\omega \rightarrow 0} \omega \sigma_2(\omega)$, as a function of pump-probe time delay τ . Data are reported for different pump pulse durations, shown on top of each pair of panels, for a constant peak field of 2.2 MV/cm. The red dashed lines are fits with a finite rise time and an exponential decay, while the blue horizontal lines indicate the 10 K equilibrium value of the superfluid density. The blue shaded areas represent the time delay window for which a finite coherent response was detected. Selected data in this figure were used to produce the plots in Fig. 3.

modeled with a series of Lorentz oscillators, for which the complex dielectric function is expressed as

$$\tilde{\epsilon}_{\text{HF}}(\omega) = \sum_i \frac{\Omega_{p,i}^2}{(\Omega_{0,i}^2 - \omega^2) - i\omega\Gamma_i}. \quad (\text{D1})$$

Here, $\Omega_{0,i}$, $\Omega_{p,i}$, and Γ_i are the peak frequency, plasma frequency, and damping coefficient of the i th oscillator, respectively.

The dielectric function of the two-fluid model is expressed as

$$\tilde{\epsilon}_{\text{LF}}(\omega) = \epsilon_\infty - \frac{\omega_J^2}{\omega^2} - \frac{\omega_D^2}{\omega^2 + i\Gamma_D\omega}. \quad (\text{D2})$$

Here, the free fit parameters are the Josephson plasma frequency, ω_J , which accounts for the superconducting-like response, and the Drude parameters ω_D and Γ_D , which are plasma frequency and scattering rate of the “normal” compo-

ment. The value of ϵ_{∞} was set to 4.5, according to previous literature [29].

In all fitting procedures a single set of fit parameters was always used to simultaneously reproduce the real and imaginary part of the optical conductivity, $\sigma_1(\omega)$ and $\sigma_2(\omega)$. The equilibrium spectra above T_c were modeled by keeping $\omega_J = 0$, since no superfluid is present, leaving all the other parameters free to vary. The result of these fits was used as a starting point for the transient data. In this procedure, the high-frequency terms contained in $\tilde{\epsilon}_{\text{HF}}$ were kept fixed while ω_J , ω_D , and Γ_D were left free to vary.

APPENDIX E: EXTENDED DATA SETS

In this section we report an extended data set from which the graphs in Fig. 2 and Fig. 3 were produced.

Figure 7 shows the complex optical conductivity, $\sigma_1(\omega) + i\sigma_2(\omega)$, of $\text{YBa}_2\text{Cu}_3\text{O}_{6.48}$ at $T = 100$ K in equilibrium (red) and at one selected pump-probe time delay after photoexcitation (blue circles), corresponding to the peak of the coherent response in $\sigma_2(\omega)$ (see also Fig. 8). We report data for different

mid-infrared pump pulse durations, all taken with the same peak field of 2.2 MV/cm. The $\sigma_1(\omega)$ spectra show an almost frequency-independent increase, indicative of enhanced dissipation, that will reach its maximum for longer time delay (not shown here; see Figs. 2 and 8). The imaginary conductivity, $\sigma_2(\omega)$, displays instead a $1/\omega$ -like divergence at low frequency, which saturates to a given amplitude for pump pulses longer than ~ 1 ps.

In Fig. 8 we report the dynamical evolution of $\int_{20 \text{ cm}^{-1}}^{75 \text{ cm}^{-1}} \sigma_1(\omega) d\omega$, indicative of dissipation, and $\lim_{\omega \rightarrow 0} \omega \sigma_2(\omega)$, which in a superconductor at equilibrium is proportional to the superfluid density, for six different pump pulse durations between 0.15 ps and 4.3 ps. For all data sets, after photoexcitation the $\sigma_1(\omega)$ spectral weight is enhanced and then relaxes on a timescale that clearly exceeds the pump pulse duration. A different evolution is observed instead in $\lim_{\omega \rightarrow 0} \omega \sigma_2(\omega)$, which appears to be finite only while the system is driven (blue shading). In this case, excitation with pulses longer than ~ 1 ps allows the “zero-temperature” equilibrium superfluid density to be reached (dashed horizontal line).

-
- [1] D. N. Basov and T. Timusk, *Rev. Mod. Phys.* **77**, 721 (2005).
- [2] C. C. Homes, T. Timusk, D. A. Bonn, R. Liang, and W. N. Hardy, *Phys. C (Amsterdam)* **254**, 265 (1995).
- [3] C. C. Homes, T. Timusk, D. A. Bonn, R. Liang, and W. N. Hardy, *Can. J. Phys.* **73**, 663 (1995).
- [4] D. N. Basov, S. I. Woods, A. S. Katz, E. J. Singley, R. C. Dynes, M. Xu, D. G. Hinks, C. C. Homes, and M. Strongin, *Science* **283**, 49 (1999).
- [5] D. van der Marel and A. Tsvetkov, *Czech. J. Phys.* **46**, 3165 (1996).
- [6] D. van der Marel and A. A. Tsvetkov, *Phys. Rev. B* **64**, 024530 (2001).
- [7] H. Shibata and T. Yamada, *Phys. Rev. Lett.* **81**, 3519 (1998).
- [8] T. Kakeshita, S. Uchida, K. M. Kojima, S. Adachi, S. Tajima, B. Gorshunov, and M. Dressel, *Phys. Rev. Lett.* **86**, 4140 (2001).
- [9] D. Nicoletti, P. Di Pietro, O. Limaj, P. Calvani, U. Schade, S. Ono, Y. Ando, and S. Lupi, *New J. Phys.* **13**, 123009 (2011).
- [10] W. Hu, S. Kaiser, D. Nicoletti, C. R. Hunt, I. Gierz, M. C. Hoffmann, M. Le Tacon, T. Loew, B. Keimer, and A. Cavalleri, *Nat. Mater.* **13**, 705 (2014).
- [11] S. Kaiser, C. R. Hunt, D. Nicoletti, W. Hu, I. Gierz, H. Y. Liu, M. Le Tacon, T. Loew, D. Haug, B. Keimer, and A. Cavalleri, *Phys. Rev. B* **89**, 184516 (2014).
- [12] B. Liu, M. Först, M. Fechner, D. Nicoletti, J. Porras, T. Loew, B. Keimer, and A. Cavalleri, *Phys. Rev. X* **10**, 011053 (2020).
- [13] C. R. Hunt, D. Nicoletti, S. Kaiser, D. Pröpper, T. Loew, J. Porras, B. Keimer, and A. Cavalleri, *Phys. Rev. B* **94**, 224303 (2016).
- [14] R. Mankowsky, M. Först, T. Loew, J. Porras, B. Keimer, and A. Cavalleri, *Phys. Rev. B* **91**, 094308 (2015).
- [15] R. Mankowsky, A. Subedi, M. Först, S. O. Mariager, M. Chollet, H. T. Lemke, J. S. Robinson, J. M. Glowia, M. P. Minitti, A. Frano, M. Fechner, N. A. Spaldin, T. Loew, B. Keimer, A. Georges, and A. Cavalleri, *Nature (London)* **516**, 71 (2014).
- [16] M. Först, A. Frano, S. Kaiser, R. Mankowsky, C. R. Hunt, J. J. Turner, G. L. Dakovski, M. P. Minitti, J. Robinson, T. Loew, M. Le Tacon, B. Keimer, J. P. Hill, A. Cavalleri, and S. S. Dhesi, *Phys. Rev. B* **90**, 184514 (2014).
- [17] D. Nicoletti, E. Casandruc, Y. Laplace, V. Khanna, C. R. Hunt, S. Kaiser, S. S. Dhesi, G. D. Gu, J. P. Hill, and A. Cavalleri, *Phys. Rev. B* **90**, 100503(R) (2014).
- [18] E. Casandruc, D. Nicoletti, S. Rajasekaran, Y. Laplace, V. Khanna, G. D. Gu, J. P. Hill, and A. Cavalleri, *Phys. Rev. B* **91**, 174502 (2015).
- [19] D. Nicoletti, D. Fu, O. Mehio, S. Moore, A. S. Disa, G. D. Gu, and A. Cavalleri, *Phys. Rev. Lett.* **121**, 267003 (2018).
- [20] A. von Hoegen, M. Fechner, M. Först, N. Taherian, E. Rowe, A. Ribak, J. Porras, B. Keimer, M. Michael, E. Demler, and A. Cavalleri, *Phys. Rev. X* **12**, 031008 (2022).
- [21] M. H. Michael, A. von Hoegen, M. Fechner, M. Först, A. Cavalleri, and E. Demler, *Phys. Rev. B* **102**, 174505 (2020).
- [22] M. Buzzi, G. Jotzu, A. Cavalleri, J. I. Cirac, E. A. Demler, B. I. Halperin, M. D. Lukin, T. Shi, Y. Wang, and D. Podolsky, *Phys. Rev. X* **11**, 011055 (2021).
- [23] J. I. Okamoto, A. Cavalleri, and L. Mathey, *Phys. Rev. Lett.* **117**, 227001 (2016).
- [24] S. J. Denny, S. R. Clark, Y. Laplace, A. Cavalleri, and D. Jaksch, *Phys. Rev. Lett.* **114**, 137001 (2015).
- [25] M. Budden, T. Gebert, M. Buzzi, G. Jotzu, E. Wang, T. Matsuyama, G. Meier, Y. Laplace, D. Pontiroli, M. Riccò, F. Schlawin, D. Jaksch, and A. Cavalleri, *Nat. Phys.* **17**, 611 (2021).
- [26] E. Rowe, B. Yuan, M. Buzzi, G. Jotzu, Y. Zhu, M. Fechner, M. Först, B. Liu, D. Pontiroli, M. Riccò, and A. Cavalleri, [arXiv:2301.08633](https://arxiv.org/abs/2301.08633).

- [27] J. T. Kindt and C. A. Schmuttermaer, *J. Chem. Phys.* **110**, 8589 (1999).
- [28] M. Born and E. Wolf, *Principles of Optics*, 7th ed. (Cambridge University Press, Cambridge, 1999), pp. 54–64.
- [29] D. v. d. Marel, H. J. A. Molegraaf, J. Zaanen, Z. Nussinov, F. Carbone, A. Damascelli, H. Eisaki, M. Greven, P. H. Kes, and M. Li, *Nature (London)* **425**, 271 (2003).